Available online at www.sciencedirect.com
ScienceDirect
Journal of Solid State Chemistry 180 (2007) 949–955
JOURNAL OF SOLID STATE CHEMISTRY
www.elsevier.com/locate/jssc

Synthesis and characterizations of hierarchical biomorphic titania oxide by a bio-inspired bottom-up assembly solution technique

Qun Dong[a], Huilan Su[a,*], Wei Cao[a], Di Zhang[a], Qixin Guo[b], Yijian Lai[c]

[a]State Key Lab of Metal Matrix Composites, Shanghai Jiaotong University, Shanghai 200030, PR China
[b]Department of Electrical and Electronic Engineering, Saga University, Saga 840-8502, Japan
[c]Instrumental Analysis Center, Shanghai Jiaotong University, Shanghai 200030, PR China

Received 13 October 2006; received in revised form 2 December 2006; accepted 26 December 2006
Available online 7 January 2007

Abstract

As a representative semiconductor metal oxide, hierarchical biomorphic mesoporous TiO_2 with interwoven meshwork conformation was successfully prepared using eggshell membrane (ESM) as a biotemplate by an aqueous soakage technique followed by calcination treatment. The synthesis conditions were systematically investigated by controlling the concentration, the pH value of the precursor impregnant, and so on. The nucleation, growth, and assembly into ESM-biomorphic TiO_2 in our work depended more on the functions of ESM biomacromolecules as well as the processing conditions. As-prepared TiO_2 meshwork exhibiting hierarchical porous structure with the pore size from 2 nm up to 4 μm, was composed of intersectant fibers assembled by nanocrystallites at three dimensions. Based on the researches into the N_2 adsorption–desorption isothermal and corresponding BJH pore-size distribution, the biomorphic TiO_2 would arose interesting applications in some fields such as photocatalysis, gas sensors, antistatic coating, dye-sensitized solar cells, etc. This mild method and the relevant ideas offer a feasible path to synthesize a new family of functional materials by integrating material science, chemistry, and biotechnology.

Keywords: Hierarchical; Interwoven; Porous titania; Nanocrystallite; Eggshell membrane

1. Introduction

Mesoporous titania has outstanding chemical and physical properties, and widespread applications in photovoltaics [1], photocatalysis [2], ductile ceramics [3], pigmentation [4], optics [5], and so on, which depend more on the phase and crystallite size of building particles as well as their relevant assembly. Therefore, the design of hierarchical mesoporous titania with tailored structures and morphologies would provide promising properties. However, feasible constructions of practical and functional metal oxides with hierarchical structures have currently been limited.

Nature always fascinates scientists and engineers with numerous examples of exceptionally fantastic building materials. It has long been using the bottom-up means to assemble nanomaterials from nanoscopic to macroscopic scale with sophisticated structure and ordering [6,7] that show much unique properties. Thus, a variety of bioinspired morphosynthesis strategies have been explored widely, thereinto self-assembly organic superstructures, organic additives, and/or biotemplates with complex functionalization patterns were used to construct inorganic materials with controllable morphologies [8–14].

Mimicing and replicating natural biomaterials must be one of the most potent shortcuts to construct hierarchical structures with complicated architectures [15] by mild, versatile, and feasible techniques. To attain this goal at a rudimentary level, the feasible approach should be interfacial sol–gel process [16]. In such a route, sol ingredients would undergo surface preferred gelation and interact with bio-elements including proteins, polysaccharides, and functional bioresidues. Therefore, biotemplate-directed synthesis in a colloid system proves an ideal approach to the design and construct of advanced materials with

*Corresponding author. Fax: +86 21 62822012.
E-mail address: hlsu@sjtu.edu.cn (H. Su).

0022-4596/$ - see front matter © 2007 Elsevier Inc. All rights reserved.
doi:10.1016/j.jssc.2006.12.027

predetermined physical and chemical properties. Herein, we chose a convenient biomaterial eggshell membrane (ESM) as the biotemplate, in view of the special proteins patterns and functional residues of the ESM biomacromolecules, to synthesis hierarchical interwoven titania through a sol–gel approach followed by thermal decomposition.

2. Experimental

2.1. Synthesis involving biotemplate

ESM was manually separated from the $CaCO_3$ shell of commercial eggs, washed with distilled water, and dried at room temperature. As-prepared membranes were cut into pieces about 2 cm in length, 1 cm in width, and conserved as the templates for further experimental procedures. It is similar for the natural ESM that its detailed amino acid composition (wt%) is Asp 7.05, Thr 4.80, Ser 4.32, Glu 9.98, Pro 9.34, Gly5.20, Ala 2.26, Cys 4.10, Val 5.30, Met 3.32, Ile 2.61, Leu 3.65, Tyr 1.87, Phe 1.35, His 2.97, Lys 2.98, Arg 5.93, and Trp 1.80. The interfacial sol–gel process went along as follows: titanium tetrachloride ($TiCl_4$) was added slowly (ca. 1 mL/min) into ice water under stirring to obtain 0.01, 0.02, 0.03, and 0.04 M $TiCl_4$ colloid medium, respectively. Typically, the pH values of 0.04 M $TiCl_4$ colloid media were adjusted to 1, 2, 3, and 4 by adding 1 M NaOH solution, respectively. The membranes were immersed in the above colloid media for 13 h at room temperature, then rinsed with distilled water and dried naturally to obtain Ti-ESM hybrid precursor. Then the ESM-templated hybrids were all calcined at 550 °C under air atmosphere for 1.5 h. In all cases, the resulting white sheets were obtained and stored in vacuum for further characterizations.

2.2. Characterization

The samples were analyzed with TGA in a universal V2.4F TA instruments analyzer in an oxygen atmosphere at the heating rate of 10 °C/min. X-ray diffraction (XRD) measurements were carried out on a Rigaku D/max 2550V instrument operating at a voltage of 40 kV and a current of 200 mA with Cu $K\alpha$ radiation ($\lambda = 1.5406$ Å) in the range of 20–90°. The morphologies of the samples were investigated on a HITACHI S-520 scanning electron microscope (SEM) and a FEI Sirion 200 field emission gun scanning electron microscope (FESEM) operated at an acceleration voltage of 5 kV. Transmission electron microscopy (TEM) and high-resolution transmission electron microscopy (HRTEM) images were obtained as a bright field image and examined by selected area electron diffraction (SAED), conducted on a JEOL JEM-2010 instrument operated at an acceleration voltage of 200 kV and a JEOL JEM-2100F instrument working at 200 kV accelerating voltage, respectively. The nitrogen adsorption and desorption isotherms were measured by using a Micromeritics ASAP 2010 M + C system. All the samples were degassed at 180 °C before the actual measurements. For the BJH (Barret–Joyner–Halenda model), the pore-size distribution was obtained from the analysis of the adsorption branch of the isotherms.

3. Results and discussion

3.1. TGA and XRD analysis

TGA results in Fig. 1 show that the ESM template started pyrolyzing at 200 °C and absolutely pyrolyzed by 550 °C. The ESM-templated hybrids containing titanic and titanyl precursors also decomposed around 200 °C, and 18.3% (by mass) inorganic ingredients remained when the template was completely removed at 550 °C. The pH value of the impregnant has a significant effect on the phase of TiO_2 crystalline products. The XRD patterns of the products prepared under different conditions (dipped in 0.04 M $TiCl_4$ media with different pH value, calcined at 550 °C) are given in Fig. 2. It shows that high acidity is in favor of the formation of rutile phase. When the pH value of the precursor is about 1, the product is a mixture of rutile (majority) and anatase (minor). With increasing pH to 2, the product is formed by a remixture of rutile (minor) and anatase (majority). It is evident that the content of anatase phase in the products increases with the mount of the pH value. At pH = 4, the rutile phase disappears yet the anatase phase becomes dominant. It reveals that as pH > 4, the only anatase phase could be obtained.

The concentration of $TiCl_4$ medium has direct affinity with the acidity of the impregnant. Fig. 3 shows the XRD patterns of templated hybrids immersed in the sol systems with different concentrations and calcined at 550 °C. Decreasing the concentration of $TiCl_4$ medium favors the formation of anatase TiO_2. When the concentration is tuned from 0.04 to 0.03 M, the peak intensity of rutile titania is abruptly weakened. As the concentration is

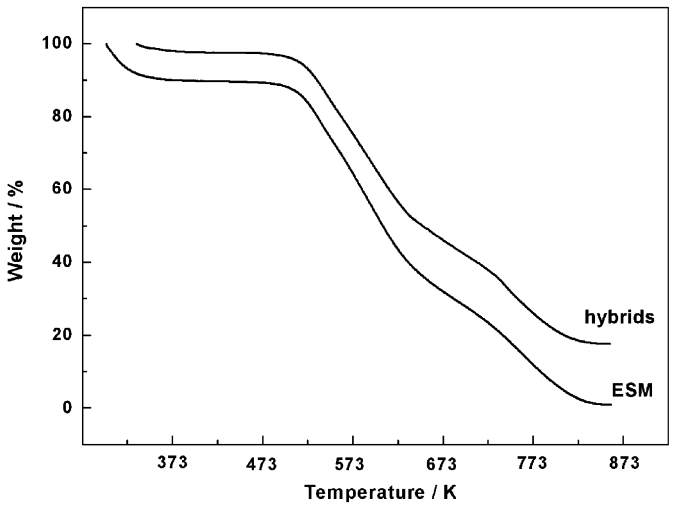

Fig. 1. TGA curves of the natural ESM and the templated Ti-ESM hybrids.

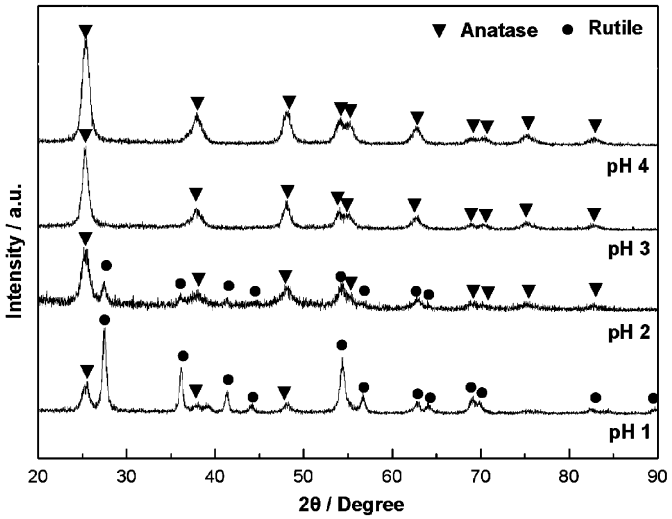

Fig. 2. XRD patterns of Ti-ESM hybrids prepared at the different medium pH value and calcined at 550 °C.

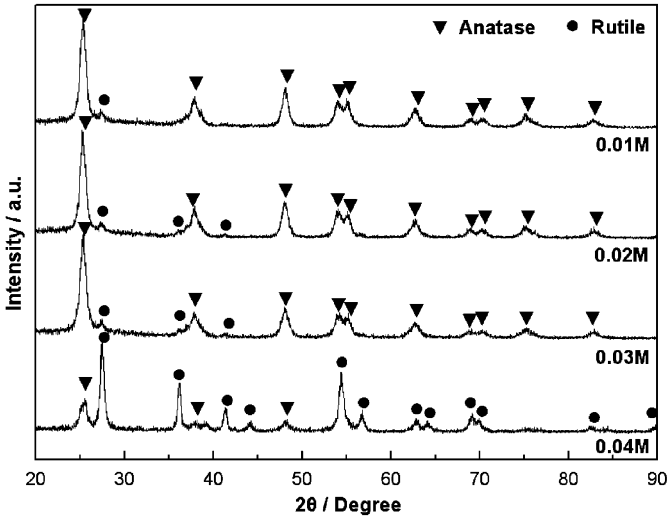

Fig. 3. XRD patterns of Ti-ESM hybrids prepared at the different medium concentration and calcined at 550 °C.

decreased to 0.02 M, further to 0.01 M, there are feeble diffraction peaks of rutile TiO_2. The above results indicate that the single anatase titania could be achieved at this concentration. All the broader reflection peaks of different samples indicate that as-prepared TiO_2 hierarchies have small dimensions. The average crystallite size of about 5–8 nm is estimated according to the line width analysis of the TiO_2 (101) diffraction peaks based on the Scherrer formula.

3.2. SEM observation

The avian eggshell is composed of multilayered membranes and calcified extracellular matrix, which are sequentially assembled during the egg moves along the oviduct [17]. The inset of Fig. 4(a) shows the SEM image of cross-fractured eggshell, it reveals that the shell membranes consist of interwoven fibers (denoted by arrows) resting upon the calcified shell which is composed of an inner mammillary layer and an outer palisade layer. In fact, ESM is a non-mineralized, collagen-based matrix between the egg white and the mineralized shell. Fig. 4(a) displays interwoven networks at large scale. Fig. 4(b) reveals the interwoven and coalescing nature of ESM fibers intercrossing one another into a meshwork at the three-dimensional model with the average fiber width ranged from 400 nm to 4 μm.

To investigate the detailed morphologies and the structures of ESM-morphic titania, representative FESEM images of the samples calcined at 550 °C are shown in Fig. 4(c–f). Fig. 4(c) indicates that the interwoven and coalescing TiO_2 fibers prepared at pH 1 and calcined at 550 °C are ranging from 0.2 to 1.5 μm in diameter in comparison with that of the original membrane fibers. Typical lowly enlarged FESEM image of this TiO_2 film displayed in inset of Fig. 4(c) reveals the integrality of the obtained sample. Although there exists considerable shrinkage, it retains the overall refined reprography of the interwoven hierarchy. At pH 2, there are some drapes engendered on the surfaces of titania fibers while the replica of ESM can also be obtained. However, when the pH value is elevated to 3, the morphology of obtained titania has a mutation. One can see from Fig. 4(d) that the titania fibers are distorted, and a sort of connected petal-shaped structure comes into being. Fig. 4(e and f) show the detailed morphologies of the biomorphic TiO_2 fibers prepared under the condition (dipped into 0.04 M or 0.01 M $TiCl_4$ impregnant, calcined at 550 °C). The two TiO_2 samples involving either 0.04 or 0.01 M $TiCl_4$ impregnant display the analogical hierarchical interwoven conformations. However, it is observed at the higher magnification that there exists the evident distinction resulted from the effects of the impregnant concentration. As shown in the insets of Fig. 4(e and f), it is more vivid that the titania fibers synthesized under higher concentration are composed of lager particles while smaller titania nanocrystallites are obtained under lower concentration. The lumpy structures may form due to the agglomeration among TiO_2 particles under the higher concentration or higher acidity of the media precursor. A careful look at the surface of the biomorphic titania reveals that some mesopores are occurred, it is more clear for the sample using 0.01 M $TiCl_4$ impregnant. The above results indicate that different morphologies of TiO_2 samples have occurred, based on the alteration of the pH value and the concentration of $TiCl_4$ impregnants.

3.3. TEM observation

The titania samples were further characterized by TEM and HRTEM results. Fig. 5(a) is the micrograph of one single fiber corresponding to pH 1 (0.04 M) and 550 °C. The porous fiber with 800 nm in diameter is assembled by

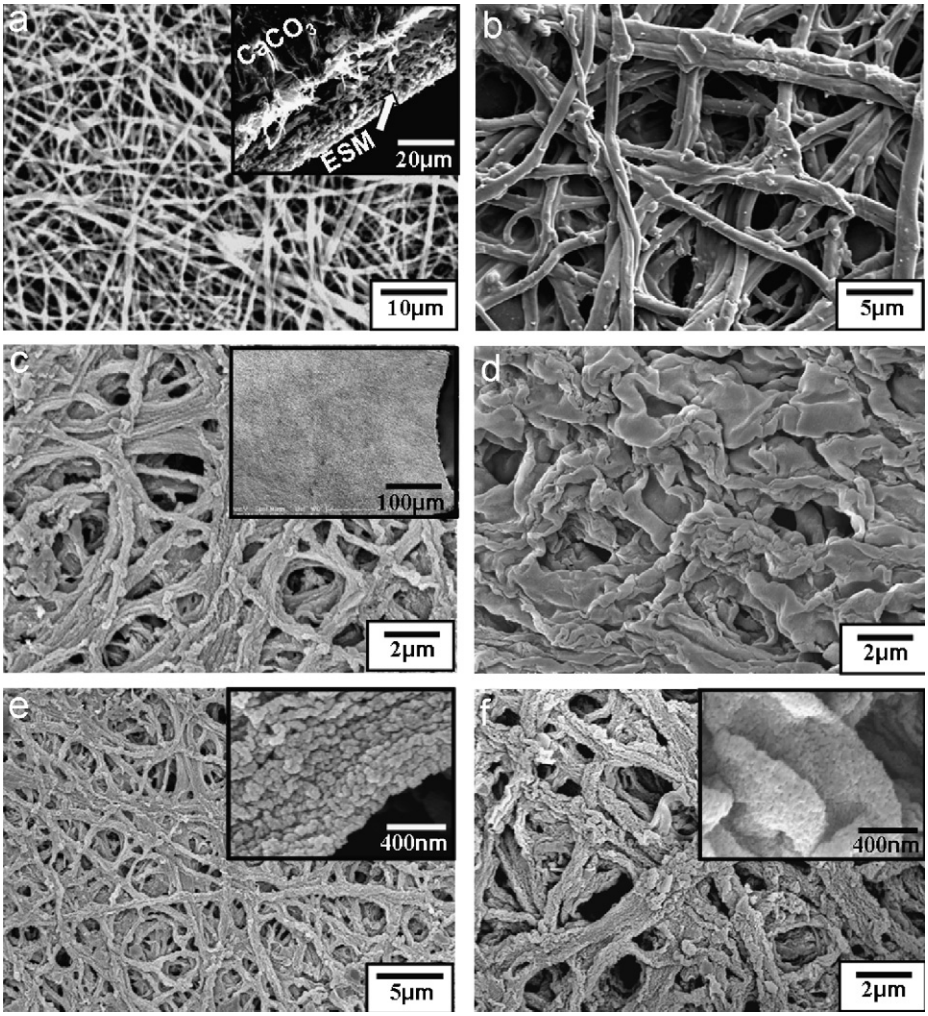

Fig. 4. (a) SEM images showing hierarchical interwoven structures of the natural ESM, inset revealing the relative distribution of $CaCO_3$ shell and the membranes; FESEM images showing (b) higher magnifications of the natural fibers; as-synthesized titania associated with the different pH value: (c) pH 1 and (d) pH 3 and the calcination temperature at 550 °C; as-synthesized titania associated with the different concentration: (e) 0.04 M and (f) 0.01 M and the calcination temperature at 550 °C. Inset in (c) displays the typical lowly enlarged SEM image of the TiO_2 film. Insets in (e) and (f) display the higher magnifications of the corresponding titania fibers, respectively.

small particles. At high magnification attained in Fig. 5(b), the titania fiber is actually assembled by the nanocrystallites with the average size of about 6 nm, which makes an allusion to the replication readily achieved by the small particles rather than large ones. The SAED patterns show that the building units of TiO_2 samples are polycrystalline nanoparticles due to the uniform central and diffraction spots, and diffraction rings are indexed to (101), (004), (200), (105), (204), and (116) diffractions of titania (insets in Fig. 5(b)), which goes well with the XRD results.

HRTEM images in Fig. 5(c and d) show the difference of TiO_2 nanocrystallites associated with the distinct pH value and the same calcination temperature 550 °C. Fig. 5(c) displaying the titania prepared at pH 2, a lattice image can be clearly seen due to the phase contrast. The distances between the adjacent lattice fringes correspond to the interplanar distances of the anatase TiO_2 (004) and rutile TiO_2 (211), which are $d_{004} = 0.238$ nm and $d_{211} = 0.170$ nm, respectively. Considering that each domain having the parallel lattice fringes is a single crystal of TiO_2, the average crystallite size is observed to be about 5–6 nm. For the sample prepared at pH 3 shown in Fig. 5(d), there is no rutile phase observed, in agreement with the XRD results. Obviously, the pH value of the colloid medium influences TiO_2 target materials greatly. The higher acidity of the collid impregnant is preferred to stabilize the ESM proteins, further to achieve the synthesis of interwoven titania. While at higher pH value, obtained titania exhibits connected petal-shaped structures. Thus tuning the pH value of the colloid system could also lead to the evolution of the morphology of hierarchical TiO_2. Since the concentration of the colloid impregnant determines the pH value, and the dilution of the nanoparticles dispersions may lead to insufficient coating, finally the building units of obtained TiO_2 were fairly small. In addition, it is notable that there are more micropores of about 2 nm observed in all the samples. It also reveals that the present TiO_2 hierarchy is characterized by the arrays of nanoparticles

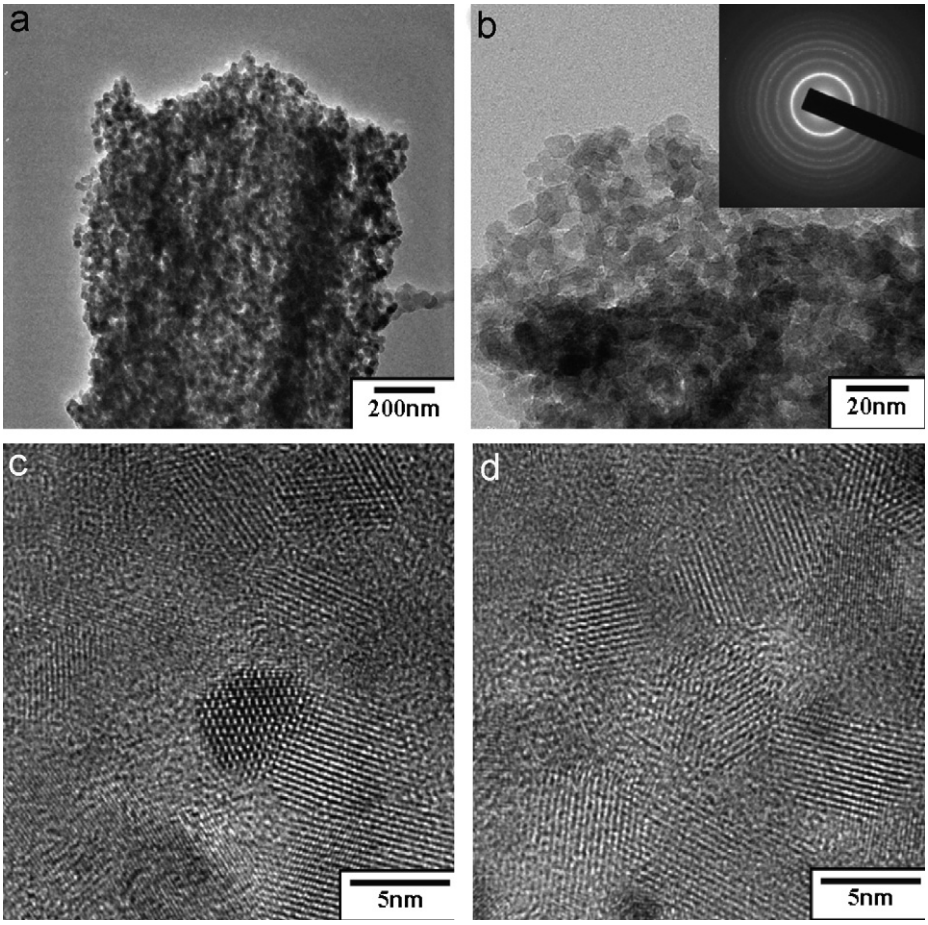

Fig. 5. TEM images of (a) an individual TiO_2 fiber; (b) the building particles of titania fibers associated with pH 1 and 550 °C. Inset in (b) shows the corresponding SAED patterns. HRTEM images of ESM-morphic TiO_2 prepared at 550 °C associated with (c) pH 2 and (d) pH 3.

consisting of the structural defects such as micropores and mesopores. It indicates that accurately defined, size-controlled TiO_2 nanoparticles of about 5 nm could be assembled to construct hierarchical nanomaterials at appropriate calcination temperature 550 °C. All in all, the synthesis conditions have momentous influence on the synthesis of the interwoven titania. The size of the assembled units is mainly effected by the medium concentration, while the morphology is dominated by the medium pH value.

The interactions between the colloids and ESM biomacromolecules present intricate and perplexing. The synthesis of biomorphic TiO_2 can be ascribed to a special sol–gel reaction involving the biotemplate ESM, during which the biomacromolecules could direct the bottom-up assembly into hierachical mesoporous titania. Analogous investigations about the mechanism have been intensively explored in our previous works [18]. The ESM glycoprotein mantle macromolecules act as the soluble species at various hierarchy levels to form templated mineral hybrids, which predefine the subtle structures of the hybrids. In such an aqueous solution, the inorganic species cross-link and polymerize to form the mesoscopically ordered inorganic/biotemplate complexes due to the self-assembly behavior of the hydrophilic groups of glycoprotein. As we know, the heat treatment frequently brings on the agglomeration and large particles. However, TiO_2 building units in our work show small size and good crystallization as well as a narrow size distribution (Fig. 6a). It probably ascribes to short-chained amino acids of glycoprotein, which functioned as the capping agents since the binding is strong enough for the control on the growth of titania nuclei [19]. For comparison, the sample is synthesized through similar sol–gel approach and calcination treatment only without involving the template, as shown in Fig. 6(b). Apparently, the above as-prepared TiO_2 is distributed mussily with the average size of 25–30 nm, while ESM-templated TiO_2 nanocrystallites with the average size of 6 nm in our work are arranged into orderly hierarchical structures, which further proves the significance of the cage effect and supports the above analysis.

3.4. N_2 adsorption measurements

Typical N_2 gas adsorption–desorption isotherms of as-synthesized hierarchical TiO_2 materials were investigated. Fig. 7(a and b) show the isotherms and the pore size distribution curves for interwoven titania prepared at pH 1, pH 2, and pH 3 (all calcined at 550 °C), respectively.

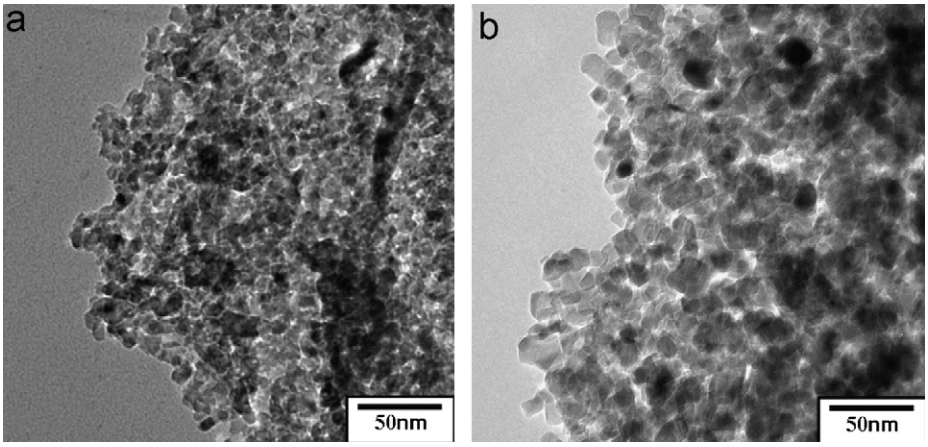

Fig. 6. TEM images of (a) ESM-based TiO_2 nanocrystallites prepared at pH 1 and 550 °C; (b) the corresponding as-synthesized TiO_2 nanoparticles without using the template through the similar process.

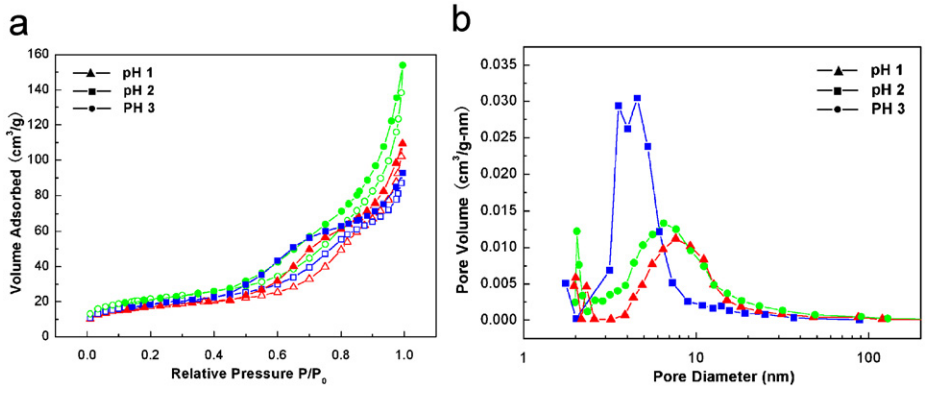

Fig. 7. (a) Nitrogen adsorption–desorption isotherms of ESM-based TiO_2 associated with different medium pH value and the same calcination temperature at 550 °C; (b) corresponding pore size distribution plots.

Table 1
Physical parameters/physisorption data of ESM-morphic TiO_2 prepared at 550 °C

Sample	pH[a]	Phase content[b]	S_{BET}[c] (m^2/g)	Pore volume[d] (ml/g^1)	Pore size[e] (nm)
A	1	(A) 20.6 (R) 79.4	60.65	0.169	9.1
B	2	(A) 63.9 (R) 36.1	65.89	0.143	6.7
C	3	(A) 100 (R) 0	74.55	0.238	10.3

[a]pH value of precursor medium.
[b]Determined by XRD, (A): anatase, (R): rutile.
[c]BET surface area calculated from the linear part of the BET plot ($P/P_0 = 0.1$–0.2).
[d]Total pore volume, taken from the volume of N_2 adsorbed at $P/P_0 = 0.995$.
[e]Average pore diameter, estimated using the desorption branch of the isotherm and the Barrett–Joyner–Halenda (BJH) formula.

The physical parameters/physisorption data of all mentioned samples are listed in Table 1. Regardless of the increase of medium pH value, the isotherms in Fig. 7(a) all exhibit IV- with H3-type hysteresis loop in the Brunauer classification [20]. As IV-type isotherm is caused by the capillary condensation of mesopores, and H3-type hysteresis loop is due to asymmetric channels and mesopores mentioned above in coincidence with the tubular characteristic pores during the synthesis process. The type of isotherms indicates an interconnected mesoporous system and very high pore connectivity according to the percolation theory [21], which goes well with the HRTEM results. The presence of a pronounced hysteresis loop in each isotherm curve is associated with the filling and emptying of mesopores by capillary condensation. At relative low pressure (<0.5), the nitrogen adsorbing action of macropores is the same as the monolayer adsorption of mesopores. But above the medium relative pressure

(>0.5), there is no capillary condensation phenomenon in macropores. Hence, according to the types of isotherms, these samples all can be confirmed as a mixture of mesopores and macropores. Here, it indicates that the pores with larger size are formed whether medium pH value higher or lower than 2 was adapted to the system. It could be reasonably ascribed to the condensation of the hydrolytic products with low acidity and contraction of frameworks with high acidity, which both bring on lager pores shown in Fig. 7(b), as demonstrated above. Herein the interwoven fibers are proved to be size-controllable porous structures. There exist several kinds of pores including micropore, mesopore, and macropore. The photocatalytic activities of the as-prepared TiO_2 fibers and the referenced P25 were examined for the decomposition of gaseous acetone. We have found that the biomorphic TiO_2 exhibited better performance than the P25. The cyclic performance of TiO_2 was also tested, and third run presented similar photocatalytic behaviors as the first run, indicating that the activity of TiO_2 was stable. However, it seems that the results (especially, catalysis efficiency) are not high as expected. Currently, we are doing repeated trials to give the precise values. The hierarchical structures along with a considerable high surface area and narrow pore size distribution are expected to have potential in catalysis, solar energy conversion, and optoelectronic devices.

4. Conclusions

Hierarchical mesoporous TiO_2 assembled by nanocrystallites units from the nanoscale to the macroscale was successfully fabricated using ESM as the biotemplate through a bio-inspired sol–gel approach. As-prepared titania shows porous characters within the range of 2 nm to 4 μm at the multiscale. The formation and assembly of hierarchical mesoporous titania rely more on calcination temperature, concentration, and pH value of the sol medium. Especially, the medium pH value in the pretreatment has great effects on the morphologies and structures, also BET surface area and their pore-size distribution of target materials. The synthesis should be under the control of glycoprotein mantle of ESM functioned as and directed by right of the interactions between ESM biomacromolecules and Ti-colloid precursors. Herein the bioinspired technique suggests materials scientists and chemists with new solutions to create superstructures resembled by naturally existing biominerals with their unusual shapes and complexity. We envisage that the exploration in these areas should provide new possibilities for the rational design of various kinds of inorganic materials with ideal hierarchy and controllable length scales, which are expected to find potential applications in more fields.

Acknowledgments

This work was supported by the financial supports of National Natural Science Foundation of China under Grant 50371055, the Major Fundamental Research Project of Shanghai Science and Technology Committee under Grant 04DZ14002, Shanghai Nanotechnology Center under Grant 05nm05020.

References

[1] B. Oregan, M. Gratzel, Nature 353 (1991) 737.
[2] H. Kominami, S. Murakami, J. Kato, Y. Kera, B. Ohtani, J. Phys. Chem. B 106 (2002) 10501.
[3] Y.F. Zhu, J.J. Shi, Z.Y. Zhang, C. Zhang, X.R. Zhang, Anal. Chem. 74 (2002) 120.
[4] C. Feldmann, Adv. Mater. 13 (2001) 1301.
[5] K.L. Frindell, M.H. Bartl, A. Popitsch, G.D. Stucky, Angew. Chem. Int. Ed. 41 (2002) 959.
[6] H.A. Lowenstam, On Biomineralization, Oxford University Press, Oxford, 1989.
[7] J. Aizenberg, J.C. Weaver, M.S. Thanawala, V.C. Sundar, D.E. Morse, P. Fratzl, Science 309 (2005) 275.
[8] R.C. Mucic, J.J. Storhoff, C.A. Mirkin, R.L. Letsinger, J. Am. Chem. Soc. 120 (1998) 12674.
[9] M. Knez, A.M. Bittner, F. Boes, C. Wege, H. Jeske, E. Maiss, K. Kern, Nano Lett. 3 (2003) 1079.
[10] R. Seshadri, F.C. Meldrum, Adv. Mater. 12 (2000) 1149.
[11] W. Zhang, D. Zhang, T.X. Fan, J. Ding, Q.X. Guo, H. Ogawa, Nanotechnology 17 (2006) 840.
[12] D. Yang, L.M. Qi, J.M. Ma., Adv. Mater. 14 (2002) 1543.
[13] Q. Dong, H.L. Su, D. Zhang, J. Phys. Chem. B 109 (2005) 17429.
[14] A.G. Dong, Y.J. Wang, Y. Tang, N. Ren, Y.H. Zhang, Y.H. Yue, Z. Gao, Adv. Mater. 14 (2002) 926.
[15] S. Mann, Biomineralization: Principles and Concepts in Bioinorganic Materials Chemistry, Oxford University Press, New York, 2001.
[16] R.A. Caruso, M. Antonietti, Chem. Mater. 13 (2001) 3272.
[17] M.S. Fernandez, M. Araya, J.L. Arias, Matrix Biol. 16 (1997) 13.
[18] H.L. Su, N. Wang, Q. Dong, D. Zhang, J. Membr. Sci. 283 (2006) 7.
[19] D.C. Pan, N.N. Zhao, Q. Wang, S.C. Jiang, X.L. Ji, L.J. An, Adv. Mater. 17 (2005) 1991.
[20] M.M. Wu, G. Lin, D.H. Chen, G.G. Wang, D. He, S.H. Feng, R.R. Xu, Chem. Mater. 14 (2002) 1974.
[21] N.A. Seaton, Chem. Eng. Sci. 46 (1991) 1895.